Contract No.:

This manuscript has been authored by Savannah River Nuclear Solutions (SRNS), LLC under Contract No. DE-AC09-08SR22470 with the U.S. Department of Energy (DOE) Office of Environmental Management (EM).

Disclaimer:

Optimization of selenium in CdZnTeSe quaternary compound for radiation detector applications

Utpal N. Roy[1*], Giuseppe S. Camarda[2], Yonggang Cui[2], and Ralph B. James[1]

[1]Savannah River National Laboratory, Aiken, SC 29808, USA
[2]Brookhaven National Laboratory, Upton, NY 11973, USA

Abstract:

X- and gamma-ray detectors are increasingly becoming essential tool for science and technology in various fields include homeland security, nonproliferation, nuclear security, medical imaging, astrophysics, and high energy physics. $Cd_{1-x}Zn_xTe_{1-y}Se_y$ (CZTS) is emerging as a next-generation compound semiconductor for such applications. CZTS was found to possesses a very low concentration of Te inclusions and free from sub-grain boundary networks. Being a quaternary compound with varying alloy composition, optimization of the composition was performed to determine the minimum amount of selenium required to produce CZTS with reduced defects. The optimized composition was found to be x=0.10 and y=0.02, i.e., $Cd_{0.9}Zn_{0.1}Te_{0.98}Se_{0.02}$, for excellent material properties as a radiation detector. The resulting material was free from sub-grain boundary networks and with a highly reduced concentration of Te inclusions. The bulk dark resistivity obtained was in the range of $1\text{-}3x10^{10}$ ohm-cm with the highest achieved mobility-lifetime product of ~$6.6x10^{-3}$ cm^2/V for the optimized CZTS composition. Impurity analyses were performed by the Glow Discharge Mass Spectroscopy (GDMS) technique, and the results showed relatively high impurity concentrations compared to commercial detector-grade CdZnTe. Thus, CZTS has room for further improvement with additional purification of the starting materials.

*Corresponding author: Utpal.Roy@srnl.doe.gov

Compact gamma and X-ray detectors operable at room temperature have experienced a long development period over about the past four decades. Because of the high penetration depth of gamma rays, it is obvious that the detector material must have a high density and a high atomic weight for the constituent elements. For more than three decades CdZnTe (CZT) has been the most successful room-temperature detector material commercially, and it has become the gold standard for R&D on alternative materials[1-7]. Despite the incremental improvements generated through intense research globally, CZT still suffers from the presence of performance-limiting defects, mostly intrinsic in nature, which are present due to the inherent poor thermophysical properties of CdTe/CZT[8]. Due to the retrograde solubility of tellurium near stoichiometry, a high concentration of Te inclusions (Te-rich secondary phases) is often found in the as-grown CdTe/CZT ingots[9,10]. The poor thermo-physical properties of the material cause appearance of high concentrations of sub-grain boundaries and their network, and often the sub-grain boundaries are decorated with Te inclusions[10,11]. Both these defects severely affect the charge transport and are also responsible for a spatial non-uniformity in the charge transport properties due to their random distribution in the CdTe/CZT matrix[12,13], eventually adversely affecting the detector performance. The presence of these performance-limiting defects greatly compromise the yield of high-quality detector grade material, while the overall yield of detector grade material from CZT ingots is also reduced due to the non-unity segregation coefficient of Zn in the CdTe matrix, which causes compositional inhomogeneity in the grown ingot[14].

Recently, we have observed that the addition of a small amount of selenium in the CZT matrix profoundly improves the material quality and successfully resolved some of the long-standing issues pertaining to CZT. The resulting quaternary compound $Cd_{1-x}Zn_xTe_{1-y}Se_y$ (CZTS) was found to be completely free from sub-grain boundary network and with highly reduced Te

inclusions[15,16]. The addition of selenium in the CZT matrix offered several other advantages over conventional CZT. The axial and radial compositional homogeneity was greatly enhanced, and higher microhardness was observed[15-17]. Enhanced homogeneity, the absence of sub-grain boundary network and the presence of reduced Te inclusions provide a higher spatial charge transport uniformity in the material and led to the emergence of high-quality detector with increased yield[16,18]. In the early phase of our research on selenium-doped CdTe alloys using Current Deep Level Transient spectroscopy (i-DLTS), we observed that selenium plays an important role in reducing the concentration of Cd vacancies in the resulting CdTeSe material. The reduction of Cd vacancies was also confirmed in detector-grade CdZnTeSe[20] through i-DLTS measurements. A reduction of the Te-inclusion concentration was also observed for Bridgman-grown CZTS[21]. Recently, Yakimov et al.[22] demonstrated a significant reduction in the density of deep-level traps in Bridgman-grown CZTS, and the device performance under high flux X-ray irradiation was reported to surpass conventional CZT. Several material properties of $Cd_{1-x}Zn_xTe_{1-y}Se_y$ have surpassed CdTe/CZT[15-18]. To achieve the best detector performance from the quaternary $Cd_{1-x}Zn_xTe_{1-y}Se_y$ compound, it is necessary to optimize the alloy composition. In this letter, we report our results to determine the optimized composition of $Cd_{1-x}Zn_xTe_{1-y}Se_y$.

Being a quaternary compound, the optimization of the composition of $Cd_{1-x}Zn_xTe_{1-y}Se_y$ is non-trivial. The complex nature of the band-gap variation of CdTeSe is an added hurdle. Although the band-gap of CdSe is higher than CdTe, because of the bowing parameter owing to the compositional disorder, the band-gap decreases below the value of CdTe with increased Se concentration up to ~ 40% Se in the composition[23]. For the quaternary $Cd_{1-x}Zn_xTe_{1-y}Se_y$, for a fixed amount of zinc, the band-gap of the compound decreases with increasing concentration of selenium following the empirical formula given below[24],

$$E_g(x,y) = 1.511 - 0.54y + 0.6x \; (x, y \leq 0.10) \; \ldots\ldots\ldots\ldots \; (1)$$

for a given concentration of selenium, the band-gap increases with increased Zn concentration. However, considering the behavior of retrograde solubility of Te for $Cd_{1-x}Zn_xTe$, adding higher zinc concentration in the compound has an adverse effect on the concentration of Te inclusions. The peak position of the solidus curve for 5% Zn concentration was found to be ~Xs=50.0155 % Te, while the corresponding values were Xs=50.03 % Te and Xs=50.074 % Te for 10% and 15% Zn composition, respectively[25]. Thus, for the ternary $Cd_{1-x}Zn_xTe$, the solidus gradually shifts along the composition axis towards Te as the ZnTe content in the solid solution increases[25]. Consequently, the concentrations of Te content (in the form of secondary phases) in $Cd_{1-x}Zn_xTe$ is expected to be higher for increased concentrations of zinc. In the present study, various compositions with selenium concentrations ranging from 1.5 atomic % to 7 atomic % have been investigated for the quaternary compound $Cd_{1-x}Zn_xTe_{1-y}Se_y$. In order to avoid the occurrence of high concentrations of secondary phases in the resulting quaternary for the compositions under investigation, a nominal 10 atomic % of Zn concentration was fixed for all samples. The resulting band-gap of the quaternary however is expected to be lower than for conventional CZT (10 atomic % Zn). Figure 1 shows the band-gap versus selenium concentration (up to 7 atomic %) calculated from the empirical formula (equation 1) for the quaternary compound $Cd_{1-x}Zn_xTe_{1-y}Se_y$ with x=0.1. Owing to the reduced band-gap with increasing selenium content, the goal of the present study was to determine the minimum amount of selenium required to obtain sub-grain boundary free $Cd_{0.9}Zn_{0.1}Te_{1-y}Se_y$ with a low concentration of secondary phases, without compromising the required high electrical resistivity.

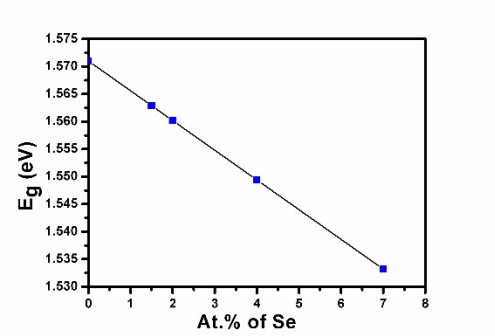

Figure 1. Band-gap of $Cd_{0.9}Zn_{0.1}Te_{1-y}Se_y$ vs. selenium concentration.

In order to study the presence of sub-grain boundaries and their network in CZTS samples, White Beam X-ray Diffraction Topography (WBXDT) measurements in the reflection mode were carried out at LBNL's ALS Beamline 3.3.2 with an X-ray beam with energy ranging from 4 keV to 25 keV. The description of the experimental setup and procedure are detailed elsewhere[15,26]. The WBXDT experiments were performed on freshly polished and etched samples in a 2% Bromine Methanol (BM) solution for two minutes. The presence of secondary phases (Te inclusions) was observed through high magnification Infra-Red (IR) transmission microscopy. Details of the IR transmission microscopic measurements were reported earlier[15,16,18]. All the measurements on CZTS samples presented here were grown by the Traveling Heater Method (THM). CZTS ingots with compositions of $Cd_{0.9}Zn_{0.1}Te_{0.93}Se_{0.07}$, $Cd_{0.9}Zn_{0.1}Te_{0.96}Se_{0.04}$, $Cd_{0.9}Zn_{0.1}Te_{0.98}Se_{0.02}$, and $Cd_{0.9}Zn_{0.1}Te_{0.985}Se_{0.015}$ and diameters of about two inch were grown by the THM following the same growth parameters using Te as the solvent. Details of THM growth conditions have been discussed earlier[16]. The charge transport characteristics such as the resistivity and mobility-lifetime product for electrons $[(\mu\tau)_e]$ have been evaluated for the CZTS samples for all the compositions mentioned above. Details of the I-V characteristics measurements and estimation of $(\mu\tau)_e$ are available in Refs. 16, 18 and 27.

Figure 2a and 2b show an optical photograph of the as-grown $Cd_{0.9}Zn_{0.1}Te_{0.93}Se_{0.07}$ sample with an area of ~1.2x1.1 cm^2 and the corresponding X-ray topographic image. As evident from the X-

ray topographic image, the sample is free from sub-grain boundaries and their network as opposed to typical CZT samples. As mentioned earlier, CZT samples in general are found to be heavily decorated with sub-grain boundary networks as observed by X-ray topographic images. A drastic reduction of Te inclusions in the $Cd_{0.9}Zn_{0.1}Te_{0.93}Se_{0.07}$ matrix was also observed as depicted in Figure 2b and 2c. The figures show the IR transmission microscopic images at two different magnifications. Selenium was also found to be effective in reducing the Te inclusions in the CdTe matrix[28]. A reduced amount of Te inclusions in Bridgman-grown CZTS ingots has

(a) **(b)** **(c)** **(d)**

Figure 2. a) Optical photograph and b) the corresponding X-ray topographic image of an as-grown $Cd_{0.9}Zn_{0.1}Te_{0.93}Se_{0.07}$ sample. Sample dimensions: ~1.2x1.1 cm^2, c) and d) IR transmission microscopic image of the as-grown $Cd_{0.9}Zn_{0.1}Te_{0.93}Se_{0.07}$ sample at two different magnifications.

also been reported recently[21]. A similar effect was also observed for 4% selenium in THM-grown CZTS ingots. Figure 3a and 3b show an optical photograph of the $Cd_{0.9}Zn_{0.1}Te_{0.96}Se_{0.04}$ sample and the corresponding X-ray topographic image with an exposed area of ~1.2x0.9 cm^2. As evident from the X-ray topographic image of the sample shown in Fig. 3b, the as-grown $Cd_{0.9}Zn_{0.1}Te_{0.96}Se_{0.04}$ material does not show the presence of any sub-grain boundaries and their network. The CZTS compound containing 4% selenium also exhibited the presence of very few Te inclusions as observed through IR transmission microscopic images shown in Fig. 3c and 3d.

(a) (b) (c) (d)

Figure 3. a) Optical photograph and b) the corresponding X-ray topographic image of an as-grown $Cd_{0.9}Zn_{0.1}Te_{0.96}Se_{0.04}$ sample. Sample dimensions: ~1.2x0.9 cm^2 (exposed area). The exposed area is the region denoted by the white rectangle (not to the scale), c) and d) IR transmission microscopic image of the as-grown $Cd_{0.9}Zn_{0.1}Te_{0.96}Se_{0.04}$ sample at two different magnifications.

Figures 4a and 5a show optical photographs of as-grown $Cd_{0.9}Zn_{0.1}Te_{0.98}Se_{0.02}$ and $Cd_{0.9}Zn_{0.1}Te_{0.985}Se_{0.015}$ samples and the corresponding X-ray topographic images (Fig. 4b and 5b) of the area denoted by the white rectangles as shown in figures 4a and 5a, respectively. The photographs of the samples shown in figures 4a and 5a were taken after lapping to show the presence of grain boundaries in the samples. The X-ray topographic measurements however were taken on polished samples followed by etching in 2% BM solution for two minutes. The optical photograph of the $Cd_{0.9}Zn_{0.1}Te_{0.98}Se_{0.02}$ sample shown in Fig. 4a contains two grains, and the X-ray topographic picture (Fig. 4b) depicts microstructural characteristics of the corresponding two grains. No sub-grain boundary or their network was observed as is evident in

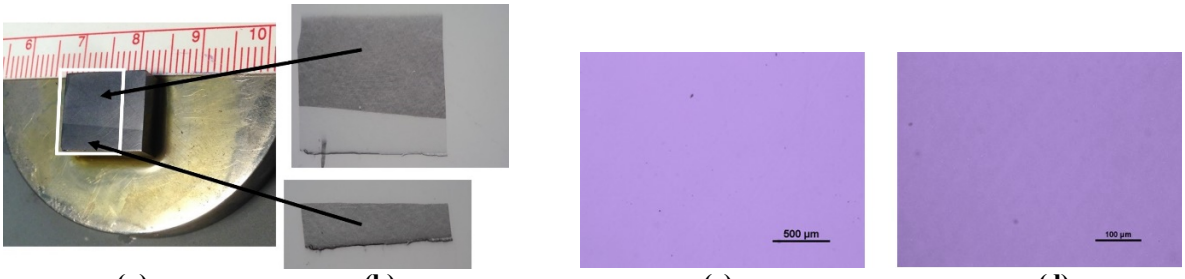

(a) (b) (c) (d)

Figure 4. a) Optical photograph and b) the corresponding X-ray topographic image of the as-grown $Cd_{0.9}Zn_{0.1}Te_{0.98}Se_{0.02}$ sample. Sample dimensions: ~1.4x1.25 cm^2. The exposed area is the region denoted by the white rectangle (not to the scale), c) and d) IR transmission microscopic image of the as-grown $Cd_{0.9}Zn_{0.1}Te_{0.98}Se_{0.02}$ sample at two different magnifications.

Fig. 4b. The CZTS sample containing 1.5% selenium was also found to be free from sub-grain boundaries and their network (see Fig. 5a and 5b). It is thus apparent that for the compositions

studied in the present investigation, the CZTS samples were free from the deleterious defects caused by sub-grain boundary networks. Although the absence of sub-grain boundaries was observed for all the compositions (7% Se to 1.5% Se), the occasional presence of isolated sub-grain boundaries was observed in some samples as reported earlier[15,16,18,27].

Selenium with a concentration as low as 1.5% to 7% in CZT matrix plays a vital role as an effective solid solution hardening agent, and it is successful in arresting the formation of sub-grain boundaries and their networks. Rudolph[10] also reported CdTeSe with 0.4% selenium was free from a sub-grain boundary network. The as-grown $Cd_{0.9}Zn_{0.1}Te_{0.98}Se_{0.02}$ samples were also found to contain much lower amounts of Te inclusions, which is consistent with our observations as shown in Fig. 4c and 4d. Higher concentrations of Te inclusions were observed for CZTS alloys containing 1.5% selenium (as shown in Fig. 5c and 5d), which was comparable to conventional CZT. The Te inclusions were observed to be distributed somewhat uniformly for large-volume detector samples[30]. While all the CZTS samples with selenium concentrations ranging from 1.5% to 7% were observed to be free from sub-grain boundary networks, the CZTS compound with 1.5% Se showed a much higher concentration of Te inclusions. A drastic reduction in the concentration of Te inclusions for CZTS samples containing 2% Se and above was observed. This reduction of Te inclusions was also observed earlier in $CdTe_{0.9}Se_{0.1}$[28]. Selenium is believed to be responsible for reducing the bulging of the retrograde solidus line near stoichiometry, which reduces the concentration of Te-rich secondary phases. From the present observation, 1.5% selenium is perhaps not effective in reducing the bulging of the retrograde solidus line to an acceptable level, hence it results in the occurrence of a higher concentration of Te inclusions. As far as sub-grain boundaries and their network and Te inclusions are concerned, $Cd_{1-x}Zn_xTe_{1-y}Se_y$ compositions with $y \geq 0.02$ contain extremely low

density of defects with surprisingly high defect tolerance. As mentioned earlier, since the band-gap energy decreases with increasing concentration of selenium in the $Cd_{0.9}Zn_{0.1}Te$ matrix, the goal is to optimize the minimum amount of selenium required to produce CZTS material free from sub-grain boundary network with reduced Te inclusions. Based on the present observation, 2% Se in $Cd_{0.9}Zn_{0.1}Te$ was found to be the optimum composition for producing CZTS with highly reduced performance-limiting defects, and this alloy composition successfully resolves many of the long-lasting material issues affecting conventional CZT.

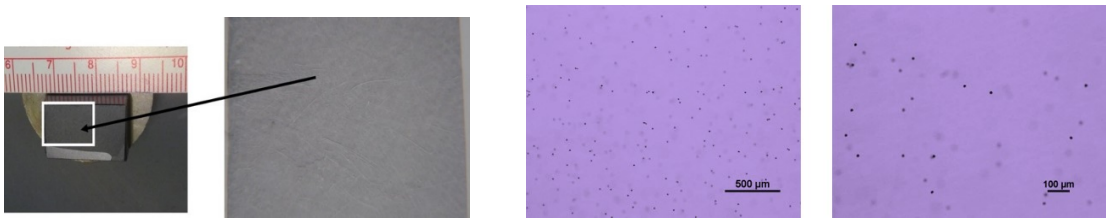

(a) (b) (c) (d)

Figure 5. a) Optical photograph and b) the corresponding X-ray topographic image of the area within the white rectangle (not to the scale) of the as-grown $Cd_{0.9}Zn_{0.1}Te_{0.985}Se_{0.015}$ sample. Sample dimensions: ~1.9x1.3 cm^2, c) and d) IR transmission microscopic image of the as-grown $Cd_{0.9}Zn_{0.1}Te_{0.985}Se_{0.015}$ sample at two different magnifications.

For detector applications the charge-transport characteristics are perhaps the most important material properties. Table 1 summarizes the resistivity and $\mu\tau$ values for electrons $[(\mu\tau)_e]$ for different compositions of CZTS with selenium concentrations ranging from 1.5% to 7%. The achieved resistivities for $Cd_{0.9}Zn_{0.1}Te_{0.98}Se_{0.02}$ and $Cd_{0.9}Zn_{0.1}Te_{0.985}Se_{0.015}$ were 1-3x10^{10} ohm-cm, which satisfies the minimum requirement for realizing detectors with low dark current and associated low noise. Although the band-gap energy is compromised for CZTS compounds as compared to $Cd_{0.9}Zn_{0.1}Te$, CZTS with selenium concentrations of 1.5% and 2% attained an acceptable level of resistivity. The resistivity obtained for $Cd_{0.9}Zn_{0.1}Te_{0.96}Se_{0.04}$ was 1-1.5x10^{10} ohm-cm, while the value was only 2-5x10^{9} ohm-cm for CZTS with 7% selenium. The reduced resistivities with higher concentrations of selenium are expected as the band-gap decreases with

increased selenium. The μτ values for electrons were estimated to be 1-2x10^{-3} cm^2/V for $Cd_{0.9}Zn_{0.1}Te_{0.985}Se_{0.015}$. The μτ values for electrons was found to be the highest for $Cd_{0.9}Zn_{0.1}Te_{0.98}Se_{0.02}$. The average $\mu\tau_e$ value obtained for the composition with 2% selenium was 4.5-5x10^{-3} cm^2/V, and the highest value achieved was ~6.6x10^{-3} cm^2/V. The lower $\mu\tau_e$ value (1-2x10^{-3} cm^2/V) for $Cd_{0.9}Zn_{0.1}Te_{0.985}Se_{0.015}$ as compared to $Cd_{0.9}Zn_{0.1}Te_{0.98}Se_{0.02}$ might be due to the presence of a higher concentration of Te inclusions in $Cd_{0.9}Zn_{0.1}Te_{0.985}Se_{0.015}$. The $\mu\tau_e$ values were observed to be very consistent for different ingots grown with the same composition. For example, the $\mu\tau_e$ values for three different ingots of $Cd_{0.9}Zn_{0.1}Te_{0.98}Se_{0.02}$ were found to be in the range mentioned in table 1. In terms of the charge-transport characteristics, the composition with 2% Se ($Cd_{0.9}Zn_{0.1}Te_{0.98}Se_{0.02}$) was found to be the best. Thus, the composition with 2% Se ($Cd_{0.9}Zn_{0.1}Te_{0.98}Se_{0.02}$) was found to be optimum in terms of the charge-transport characteristics, as well as the microstructure and Te-rich secondary phases. It is worth mentioning here that despite dramatic improvements in material quality with a highly reduced concentration of performance-limiting defects, the $(\mu\tau)_e$ values for CZTS (2% Se) samples are at least 5-7 times lower than that for high quality commercial-grade CZT. Recently, a $(\mu\tau)_e$ value of 6.4×10^{-4} cm^2/V was reported[29] for modified vertical Bridgman grown $Cd_{0.9}Zn_{0.1}Te_{0.97}Se_{0.03}$. The presence of a relatively high concentration of extrinsic impurities in CZTS was confirmed by Glow Discharge Mass Spectroscopy (GDMS), and these impurities are believed to be the limiting cause of the lower mobility-lifetime values in CZTS for Se concentrations over ~2%. Table 2 lists some of the detrimental impurities present in a typical THM-grown $Cd_{0.9}Zn_{0.1}Te_{0.98}Se_{0.02}$ ingot. Most of these impurities were found to be undetectable in commercial-grade THM grown CZT, as analyzed by GDMS technique except for Fe (at 22 ppba)[30]. Most of the measured

Table 1. Resistivity and $(\mu\tau)_e$ values for CZTS with different selenium concentrations.

Composition	Resistivity (Ω-cm)	$(\mu\tau)_e$ (cm^2/V)
$Cd_{0.9}Zn_{0.1}Te_{0.93}Se_{0.07}$	$2\text{-}5x10^9$	$1\text{-}2x10^{-3}$
$Cd_{0.9}Zn_{0.1}Te_{0.96}Se_{0.04}$	$1\text{-}1.5x10^{10}$	$2\text{-}2.5x10^{-3}$
$Cd_{0.9}Zn_{0.1}Te_{0.98}Se_{0.02}$	$1\text{-}3x10^{10}$	$6.6x10^{-3}$ (highest) $4.5\text{-}5\ x10^{-3}$ (average)
$Cd_{0.9}Zn_{0.1}Te_{0.985}Se_{0.015}$	$1\text{-}3x10^{10}$	$1\text{-}2x10^{-3}$

impurities in the THM-grown $Cd_{0.9}Zn_{0.1}Te_{0.98}Se_{0.02}$ ingot was found to be even higher than the impurities present in CdZnTe starting material. It is thus obvious that the source of these relatively high concentrations of impurities is the CdSe starting material. The lower values of mobility-life time product for electrons in $Cd_{0.9}Zn_{0.1}Te_{0.93}Se_{0.07}$ and $Cd_{0.9}Zn_{0.1}Te_{0.96}Se_{0.04}$ can thus be explained due to the presence of higher impurity content for increased levels of selenium in the compound. It is to be noted that even with the presence of relatively high concentrations of the detrimental impurities and lower $(\mu\tau)_e$ values for CZTS (5- $6.6x10^{-3}$ cm^2/V), we achieved an as-measured energy resolution of 1.0±0.1% at 662 keV for 1-cm long Frisch grid detectors[16,18]. For CZT, a similar energy resolution could be achieved for material having $(\mu\tau)_e$ value > 10^{-2} cm^2/V[31]. Thus, achieving a remarkable energy resolution with moderate $(\mu\tau)_e$ value for CZTS is due to the dramatic improvement of the charge-transport uniformity, overall microstructural quality and reduction of other performance limiting defects (e.g., Te inclusions). It is thus apparent that the $(\mu\tau)_e$ value and the resulting detector response can further be improved by reducing the detrimental extrinsic impurities using better purification of the starting materials for the THM growth of CZTS.

Table 2. Selected impurity concentrations present in THM-grown $Cd_{0.9}Zn_{0.1}Te_{0.98}Se_{0.02}$ ingot as measured by GDMS.

Elements	Concentration [ppb at.]
Cr	36
Fe	42
Ni	16
Cu	<4
Sn	<100
Pb	11

In this report we have investigated the structural defects and charge transport properties for different selenium concentration in CZTS compounds grown by the THM technique to achieve optimized CZTS crystals with highly reduced performance-limiting defects for radiation detector applications. The selenium concentration was varied over the range of 1.5 to 7 atomic %, while keeping the Zn concentration at a value of 10 atomic% for all CZTS compositions. The presence of sub-grain boundaries and their networks and the concentration of Te inclusions were studied by X-ray topography and IR transmission microscopy, respectively. The optimized CZTS compound was achieved with a 2 atomic% selenium. All the compositions investigated were found to be free from sub-grain boundary networks. Additionally, the minimum amount of selenium of 2 atomic % in CZTS compound was found to contain the least Te-rich inclusions. Measurements of the charge-transport characteristics revealed that the same 2 atomic % selenium in CZTS matrix was also optimum for charge collection and detector performance. Using GDMS measurements the impurity concentrations in CZTS were found to be much higher than commercial detector grade CZT. The present study suggests that after better purification of the starting material, CZTS crystals with reduced impurity concentrations can be further improved with corresponding improvements in the $(\mu\tau)_e$ values and detector energy resolution. Because of

these promising observations of highly reduced defects, $Cd_{0.9}Zn_{0.1}Te_{0.98}Se_{0.02}$ was demonstrated as a potential candidate to replace the present day CZT material.

Acknowledgements

This work was supported primarily by the U.S. Department of Energy, Office of Defense Nuclear Nonproliferation Research and Development. The author UNR acknowledges partial support by the Laboratory Directed Research and Development (LDRD) program within the Savannah River National Laboratory (SRNL). This document was prepared in conjunction with work accomplished under Contract No. DE-AC09-08SR22470 with the U.S. Department of Energy (DOE) Office of Environmental Management (EM).

Data Availability: The data on these findings are available from authors upon reasonable request.

References:

1. T. E. Schlesinger, J. E. Toney, H. Yoon, E. Y. Lee, B. A. Brunett, L. Franks, and R. B. James, Materials Science and Engineering **R 32**, 103 (2001).

2. G. Yang and R. B. James, "*Applications of CdTe, CdZnTe, and CdMnTe Radiation Detectors"*, Physics, Defects, Hetero- and Nano-structures, Crystal Growth, Surfaces and Applications Part II, edited by R. Triboulet (Elsevier, 2009) 214.

3. R. Triboulet, Phys. Status. Solidi **(c) 5**, 1556 (2005).

4. C. Szeles, IEEE Trans. Nucl. Sci. **51**, 1242 (2004).

5. H. Chen, S. A. Awadalla, J. Mackenzie, R. Redden, G. Bindley, A. E. Bolotnikov, G. S. Camarda, G. Carini, and R. B. James, IEEE Trans. Nucl. Sci. **54**, 811 (2007).

6. J. MacKenzie, F. J. Kumar, and H. Chen, J. Elect. Materials 42, 3129 (2013).

7. U. N. Roy, A. Gueorguiev, S. Weiller, and J. Stein, J. Cryst. Growth **312**, 33 (2009).

8. P. Rudolph, Cryst. Res. Technol. **40**, 7 (2005).

9. A. E. Bolotnikov, O. S. Babalola, G. S. Camarda, Y. Cui, S. U. Egarievwe, R. Hawrami, A. Hossain, G. Yang, and R. B. James, IEEE Trans. Nucl. Sci. **57**, 910 (2010).

10. P. Rudolph, Prog. Crystal Growth and Charact. **29**, 275 (1994).

11. A. E. Bolotnikov, G. S. Camarda, Y. Cui, G. Yang, A. Hossain, K. Kim, and R. B. James, J. Cryst. Growth **379**, 46 (2013).

12. G. S. Camarda, A. E. Bolotnikov, Y. Cui, A.Hossain, S. A. Awadalla, J. Mackenzie, H. Chen, and R. B. James, IEEE Trans. on Nucl. Sc. **55**, 3725 (2008).

13. G. A. Carini, A. E. Bolotnikov, G. S. Camarda, and R. B. James, Nucl. Instrum. Methods **A 579**, 120 (2007).

14. N. Zhang, A. Yeckel, A. Burger, Y. Cui, K.G. Lynn, and J. J. Derby, J. Cryst. Growth **325**, 10 (2011).

15. U. N. Roy, G. S. Camarda, Y. Cui, R. Gul, A. Hossain, G. Yang, J. Zazvorka, V. Dědič, J. Franc, and R. B. James, Sci. Rep. **9**, 1620 (2019).

16. U. N. Roy, G. S. Camarda, Y. Cui, R. Gul, G. Yang, J. Zazvorka, V. Dědič, J. Franc, and R. B. James, Sci. Rep. **9**, 7303 (2019).

17. J. Franc, P. Moravec, V. Dědič, U. Roy, H. Elhadidy, P. Minárika, V. Šíma, Materials Today Communications **24**, 101014 (2020).

18. U. N. Roy, G. S. Camarda, Y. Cui, and R. B. James, Appl. Phys. Lett. **114**, 232107 (2019).

19. R. Gul, U. N. Roy, A. E. Bolotnikov, G. S. Camarda, Y. Cui, A. Hossain, W. Lee, G. Yang, Y. Cui, A. Burger, and R. B. James, APL Mater. **3**, 040702 (2015).

20. R. Gul, U. N. Roy, G. S. Camarda, A. Hossain, G. Yang, P. Vanier, V. Lordi, J. Varley, and R. B. James, J. Appl. Phys. **121**, 125705 (2017).

21. S. Hwang, H. Yu, A. E. Bolotnikov, R. B. James, and K. Kim, IEEE Trans. on Nucl. Sc. **66**, 2329 (2019).

22. A. Yakimov, D. Smith, J. Choi, and S. Araujo, Proc. SPIE **11114**, Hard X-Ray, Gamma-Ray, and Neutron Detector Physics **XXI**, 111141N (2019).

23. L. Hannachi, and N. Bouarissa, Superlattices and Microstructures **44**, 794 (2008).

24. G. Brill, Y. Chen, P.M. Amirtharaj, W. Sarney, D. Chandler-Horowitz, and N. K. Dhar, J. Electron. Materials **34**, 655 (2005).

25. V. N. Guskov, J. H. Greenberg, M. Fiederle, K. W. Benz, J. Alloys and Comp. **371**, 118 (2004).

26. U. N. Roy, A. E. Bolotnikov, G. S. Camarda, Y. Cui, A. Hossain, K. Lee, G. Yang, and R. B. James, J. Crystal Growth **389**, 99 (2014).

27. U. N. Roy, G. S. Camarda, Y. Cui, and R. B. James, Appl. Phys. Lett. **115**, 242102 (2019).

28. U. N. Roy, A. E. Bolotnikov, G. S. Camarda, Y. Cui, A. Hossain, K. Lee, W. Lee, R. Tappero, G. Yang, R. Gul, and R. B. James, APL Materials **3**, 026102 (2015).

29. S. K. Chaudhuri, M. Sajjad, J. W. Kleppinger, and K. C. Mandal, J. Appl. Phys. **127**, 245706 (2020).

30. J. J. McCoy, S. Kakkireni, Z. H. Gilvey, S. K. Swain, A. E. Bolotnikov, and K. G. Lynn, J. Electron. Mater. **48**, 4226 (2019).

31. H. Chen, S. A. Awadalla, K. Iniewski, P. H. Lu, F. Harris, J. Mackenzie, T. Hasanen, W. Chen, R. Redden, G. Bindley, I. Kuvvetli, C. Budtz-Jørgensen, P. Luke, M. Amman, J. S. Lee, A. E. Bolotnikov, G. S. Camarda, Y. Cui, A. Hossain, and R. B. James, J. Appl. Phys. **103**, 014903 (2008).

Figure captions:

Figure 1. Band-gap of $Cd_{0.9}Zn_{0.1}Te_{1-y}Se_y$ vs. selenium concentration.

Figure 2. a) Optical photograph and b) the corresponding X-ray topographic image of an as-grown $Cd_{0.9}Zn_{0.1}Te_{0.93}Se_{0.07}$ sample. Sample dimensions: ~1.2x1.1 cm^2, c) and d) IR transmission microscopic image of the as-grown $Cd_{0.9}Zn_{0.1}Te_{0.93}Se_{0.07}$ sample at two different magnifications.

Figure 3. a) Optical photograph and b) the corresponding X-ray topographic image of an as-grown $Cd_{0.9}Zn_{0.1}Te_{0.96}Se_{0.04}$ sample. Sample dimensions: ~1.2x0.9 cm^2 (exposed area). The exposed area is the region denoted by the white rectangle (not to the scale), c) and d) IR transmission microscopic image of the as-grown $Cd_{0.9}Zn_{0.1}Te_{0.96}Se_{0.04}$ sample at two different magnifications.

Figure 4. a) Optical photograph and b) the corresponding X-ray topographic image of the as-grown $Cd_{0.9}Zn_{0.1}Te_{0.98}Se_{0.02}$ sample. Sample dimensions: ~1.4x1.25 cm^2. The exposed area is the region denoted by the white rectangle (not to the scale), c) and d) IR transmission microscopic image of the as-grown $Cd_{0.9}Zn_{0.1}Te_{0.98}Se_{0.02}$ sample at two different magnifications.

Figure 5. a) Optical photograph and b) the corresponding X-ray topographic image of the area within the white rectangle (not to the scale) of the as-grown $Cd_{0.9}Zn_{0.1}Te_{0.985}Se_{0.015}$ sample. Sample dimensions: ~1.9x1.3 cm^2, c) and d) IR transmission microscopic image of the as-grown $Cd_{0.9}Zn_{0.1}Te_{0.985}Se_{0.015}$ sample at two different magnifications.